

Noncontact Speckle Contrast Diffuse Correlation Tomography of Blood Flow Distributions in Burn Wounds: A Preliminary Study

Mingjun Zhao, PhD*; Siavash Mazdeyasna, MS*; Chong Huang, PhD*; Nneamaka Agochukwu-Nwubah, MD†; Alisha Bonaroti, MD†; Lesley Wong, MD†; Guoqiang Yu, PhD*

ABSTRACT Introduction: Tissue injuries are often associated with abnormal blood flow (BF). The ability to assess BF distributions in injured tissues enables objective evaluation of interventions and holds the potential to improve the acute management of these injuries on battlefield. Materials and Methods: We have developed a novel speckle contrast diffuse correlation tomography (scDCT) system for noncontact 3D imaging of tissue BF distributions. In scDCT, a galvo mirror was used to remotely project near-infrared point light to different source positions and an electron multiplying charge-coupled-device was used to detect boundary diffuse speckle contrasts. The normalized boundary data were then inserted into a modified Near-Infrared Fluorescence and Spectral Tomography program for 3D reconstructions of BF distributions. This article reports the first application of scDCT for noncontact 3D imaging of BF distributions in burn wounds. Results: Significant lower BF values were observed in the burned areas/volumes compared to surrounding normal tissues. Conclusions: The unique noncontact 3D imaging capability makes the scDCT applicable for intraoperative assessment of burns/wounds, without risk of infection and without interfering with sterility of the surgical field. The portable scDCT device holds the potential to be used by surgeons in combat surgical hospitals to improve the acute management of battlefield burn injuries.

INTRODUCTION

Current day life-threatening battle injuries consist of extensive soft tissue injuries from gunshot wounds, fragmentation injuries, or blast injuries.¹ Blood flow (BF) is important, as it affects the delivery of nutrients and oxygen to tissues and the cleaning of metabolic by-products from tissues. Abnormal BF can be an indicator of various types of tissue injuries.² Assessment of BF distributions in burn wounds can provide essential information on determining the necessity and the precise area that requires wound excision and skin grafting in order to ensure successful surgical outcomes. Therefore, for surgeons in combat surgical hospitals, the ability to assess BF in injured tissues could enable precise operative debridement and improve the acute management of battlefield injuries.³

Although a variety of methods have been explored for the evaluation and prediction of tissue ischemia and subsequent necrosis, none of them are ideal. Doppler ultrasound measurement is limited to the assessment of BF in large vessels. Larger

imaging systems that can assess microvascular BF include arterial-spin-labeled magnetic resonance imaging,⁴ positron emission tomography (PET),⁵ xenon-enhanced computed tomography (XeCT),⁶ perfusion computed tomography (PCT),⁷ and single photon emission computed tomography (SPECT).⁸ However, these techniques require large and expensive instrumentation and are difficult for bedside measurements in clinical settings. Furthermore, most of these techniques (PET, XeCT, PCT, and SPECT) expose patients to undue radiation risk. These limitations decrease the clinical usefulness of these modalities in the battlefield environment.

Various optical technologies have been developed and used for BF imaging. Optical instruments are generally inexpensive and portable and can be used for continuous and longitudinal monitoring of BF variations. Laser speckle contrast imaging and laser Doppler allow for BF measurements in superficial tissues with a depth less than 1 mm.^{9,10} Near-infrared (NIR) diffuse correlation tomography (DCT) images BF distributions in relatively deep tissues (up to 15 mm) with contact fiber-optic probes.¹¹ More recently, our lab has developed a noncontact DCT (ncDCT) system for BF imaging to avoid hemodynamic variations because of the probe-tissue compression and eliminate the risk of complications from the probe contact with ulcerated or wounded tissues.¹² However, DCT/ncDCT systems use expensive long coherence lasers as sources and single-photo-counting avalanche photodiodes as detectors, which increases instrument cost and size, and results in low temporal and spatial resolution.

To overcome these barriers, we recently developed a noncontact speckle contrast diffuse correlation tomography (scDCT) system, in which a galvo mirror was used to remotely

*F. Joseph Halcomb III, M.D. Department of Biomedical Engineering, University of Kentucky, 143 Graham Ave, Lexington, KY 40508

†Division of Plastic Surgery, University of Kentucky, 1000 S. Limestone, Lexington, KY 40536

Guarantor: Guoqiang Yu

Presented as a poster at the 2018 Military Health System Research Symposium, August 2018, Kissimmee, FL; abstract # MHSRS-18-1688.

The views expressed in this article are those of the authors and do not necessarily represent National Institutes of Health, American Heart Association, National Endowment for Plastic Surgery, National Science Foundation or University of the Kentucky.

doi:10.1093/milmed/usz233

© Association of Military Surgeons of the United States 2019. All rights reserved. For permissions, please e-mail: journals.permissions@oup.com.

deliver point NIR light to source positions, and an electron multiplying charge-coupled-device (EMCCD) was used to detect BF distributions in relatively deep tissues.^{13,14} Thousands of pixels provided by the EMCCD camera significantly improve the sampling density and temporal/spatial resolution and reduce the cost of the instrument. The scDCT system has been tested for 3D imaging of BF distributions in tissue-simulating phantoms, human forearms, and mastectomy skin flaps.^{13–15} Results from these measurements demonstrate that scDCT enables a fast and high-density 3D imaging of BF distributions in relatively deep tissue volumes (up to ~10 mm) over an adjustable region of interest (ROI).

In this study, we adapted this novel scDCT for noncontact 3D imaging of BF distributions in burn wounds of two patients as a proof of concept. Knowledge of BF distributions in injured tissues is essential for improving acute management of battlefield injuries in combat surgical hospitals.

METHODS

Speckle Contrast Diffuse Correlation Tomography

Figure 1 shows the principle and measurement setup of our noncontact scDCT system. Details about noncontact scDCT system can be found from our previous publications.^{12–15} Briefly, point-source NIR light from a long coherence laser (830 nm, CrystaLaser) was delivered through a multimode fiber (core size: 200 microns) to an achromatic lens (AC127–019-B, Thorlabs) and then to a galvo mirror (GVS002, Thorlabs). The galvo mirror projected NIR light to different source positions in a selected ROI. A highly sensitive EMCCD (Cascade 1 K, Photometrics) was used to detect boundary diffuse speckle contrasts in the ROI, with a typical exposure time of 5 ms. A zoom lens (Zoom 7000, Navitar) was connected to the EMCCD camera enabling easy adjustment of ROI size. A pair of polarizers (LPNIRE050-B and LPNIRE200-B, Thorlabs) was added across the source light path and EMCCD detection path to reduce the light source reflection from the tissue surface. A long-pass filter (>750 nm, #84–761, EdmundOptics) was added in front of the zoom lens to minimize the influence of ambient light in the operating room.

The scDCT system was assembled on a mobile cart (Fig. 1a). The EMCCD camera could be easily adjusted with the articulated arm seating on top of the cart to focus on a selected ROI. The scDCT system was automatically controlled by a custom-made LabView program with a user-friendly graphic interface for data collection. Currently, the scDCT system needed a plug-in power supply.

Experimental Protocols

The experimental protocol was approved by the University of Kentucky Institutional Review Board (IRB #43961). Three patients with full thickness burn wounds were enrolled in this study to test the feasibility of scDCT technology for noncontact 3D imaging of BF distributions. This article reported only

two patients who were imaged under anesthesia in the operating room. For both patients, BF images were acquired by scDCT before wound excision and grafting (Fig. 1c). Imaging of the third patient was performed at the inpatient department under conscious conditions. Unfortunately, the measurement was contaminated by motion artifacts because of the subject movement during data collection. Therefore, this patient was excluded from data analysis.

A ROI of 80 × 80 mm was selected to cover an area with wound tissue and some adjacent normal tissues. The 9 × 9 sources separated by 1 cm of each were used to evenly cover the ROI (Fig. 1d). Data collection time ranged from several seconds to several minutes depending on the selected ROI size and sampling density. Larger ROI and higher sampling density required more time for data collection. In the present study, data acquisition time over a ROI of 80 × 80 mm was set as ~1.5 minutes.

Data Processing and BF Image Reconstruction

Details about data processing and BF image reconstruction can be found in our previous publications.^{12–15} Briefly, raw EMCCD images were first preprocessed to correct dark and shot noises and image distortion because of the smear effect. Spatial speckle contrast (K_s) detected by the EMCCD at a distance r from the source location was calculated as $K_s(r) = \sigma_s / \langle I \rangle$, where σ_s is the spatial standard deviation of light intensity and $\langle I \rangle$ is the mean intensity in a pixel window of 7 × 7 pixels. For this study, 41 × 41 detectors were evenly defined over the ROI, separated by 2 mm each (Fig. 1d). Each detector region was defined as binding 3 × 3 adjacent pixel windows. The boundary $K_s(r)$ at each S-D pair was calculated by averaging $K_s(r)$ over each detector and over two frame images to enhance the signal-to-noise ratio.

The $K_s(r)$ is a function of blood flow index [BFI(r)] and other optical properties such as tissue absorption coefficient (μ_a) and reduced scattering coefficient (μ'_s), which can be measured by other techniques (eg, NIR spectroscopies) or assumed from the literature.¹⁶ The boundary BFI(r) data were normalized to their mean value (assigning “1”) to calculate the relative BF (rBF). The normalized boundary rBF(r) data at the S-D separations ranging from 7 to 19 mm were then inserted into a modified Near-Infrared Fluorescence and Spectral Tomography (NIRFAST) program for 3D tomographic reconstructions of BF distributions in the targeted tissue volume.¹² A slab shape tetrahedral mesh with a volume of 100 × 100 × 30 mm³ and a node distance of 2 mm was created for 3D image reconstruction of BF distributions. The image reconstruction and display were performed off-line.

RESULTS

Figure 2 shows the imaging results from Patient 1. Figure 2a shows the surface color photo of the selected ROI that covers the areas of full thickness burn, partial thickness

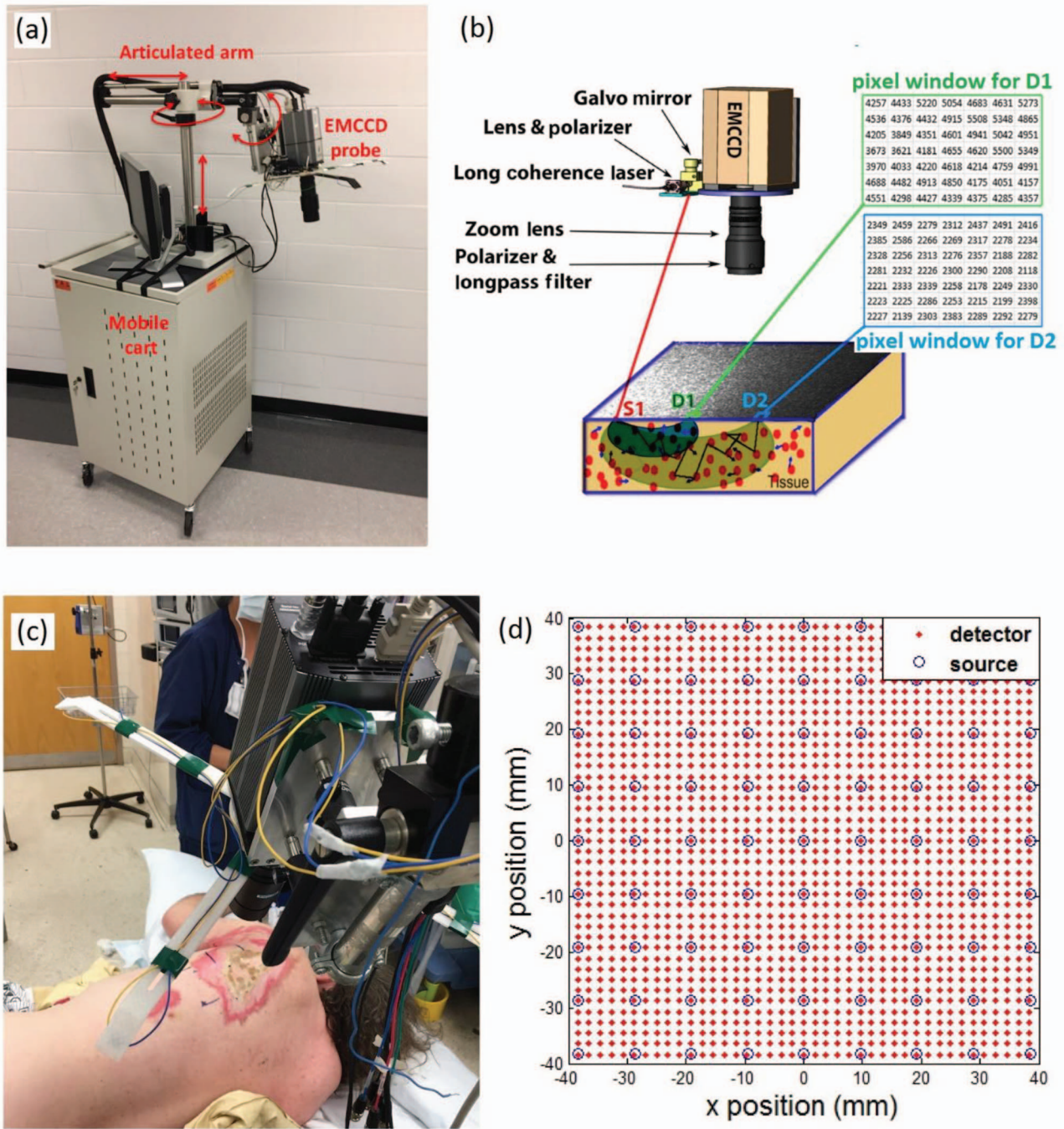


FIGURE 1. Noncontact scDCT System for 3D Imaging of BF Distributions. (a) The scDCT system was assembled on a mobile cart. (b) The principle of scDCT. (c) 3D imaging of BF distribution in burn wounds. (d) The source-detector arrangement in the selected ROI.

burn, and the surrounding normal tissue. The boundaries across the burned and normal tissues are marked with blue lines. Figure 2b shows the reconstructed 2D cross-section views of rBF distributions in the targeted tissue at different depths of 0, 3, 6, and 9 mm below the skin surface. The average rBF values in the full thickness burn volume, the partial thickness burn volume, and the normal tissue

volume were 0.97 ± 0.054 , 1.01 ± 0.053 , and 1.04 ± 0.062 (mean \pm standard deviation), respectively (Fig. 2c). One-way analysis of variance (ANOVA) test revealed significant differences in rBF among different tissue volumes ($p < 0.001$). Posthoc tests in ANOVA suggested significant differences in rBF for each pair-wise comparison across different tissue volumes ($p < 0.001$).

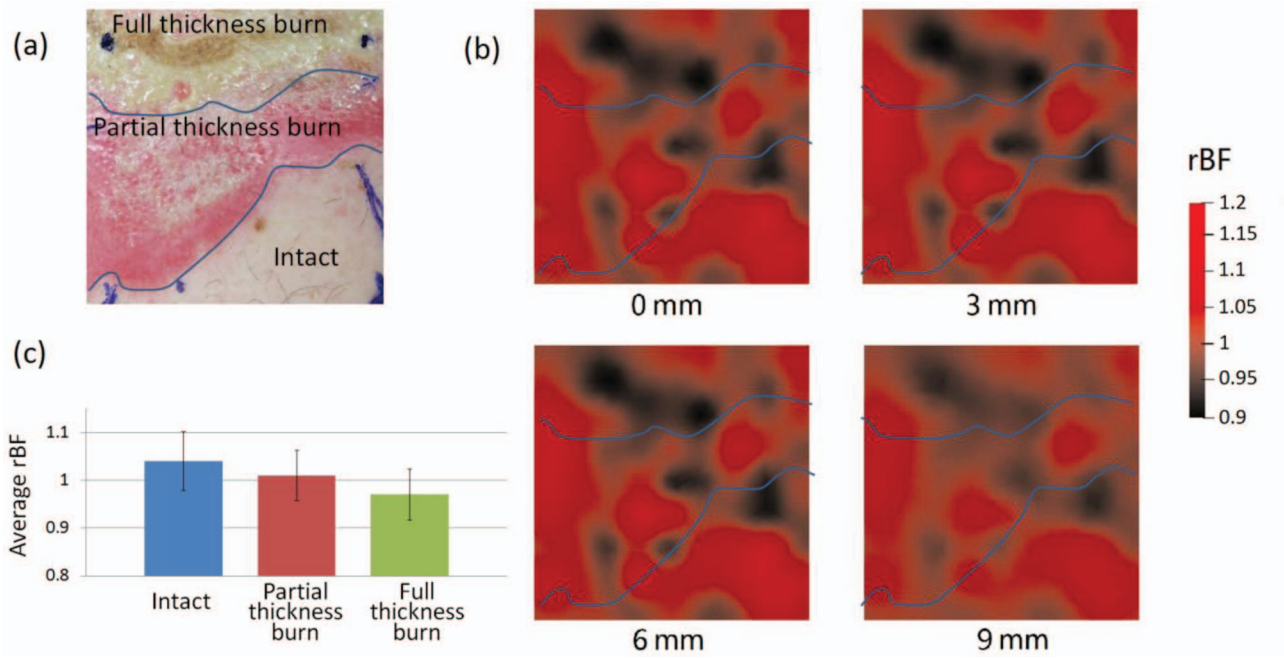


FIGURE 2. BF Distributions in Patient 1. (a) A photo of the selected ROI. (b) 2D cross-section views of rBF distributions at the depths of 0, 3, 6, and 9 mm. (c) A bar graph to show average rBF values in different tissue volumes. Error bars represent standard deviations.

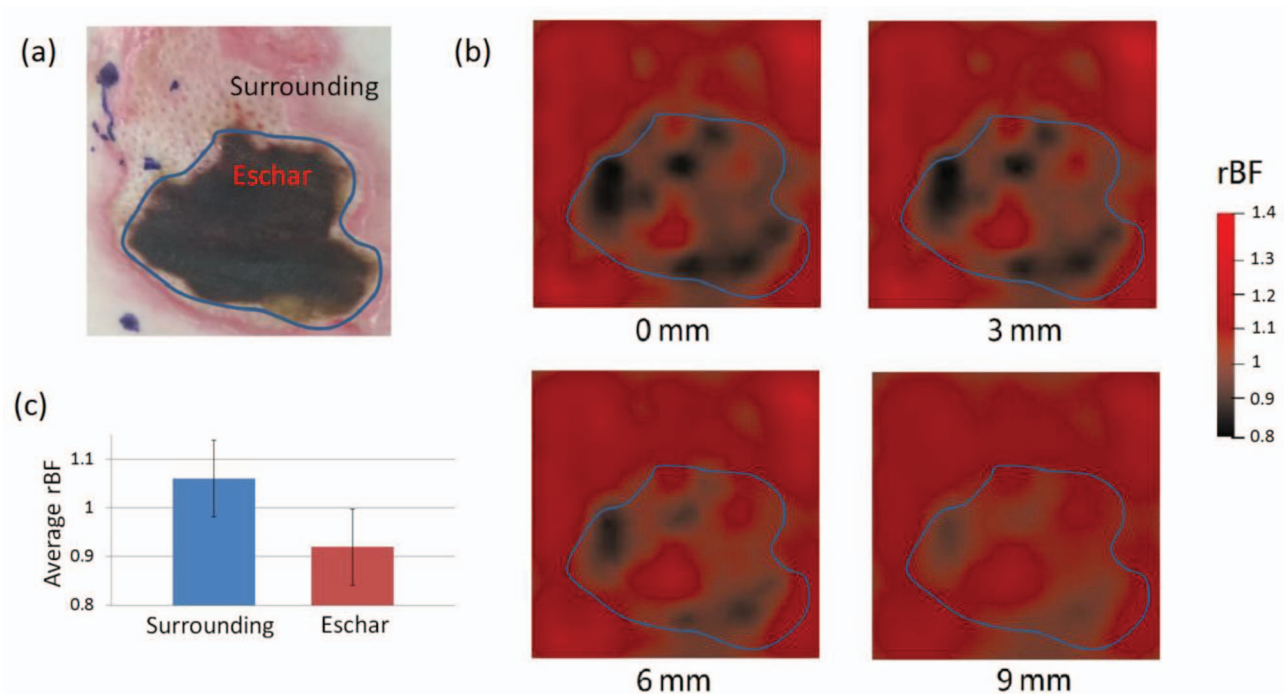


FIGURE 3. BF Distributions in Patient 2. (a) A photo of the selected ROI. (b) 2D cross-section views of rBF distributions at the depths of 0, 3, 6, and 9 mm. (c) A bar graph to show average rBF values in different tissue volumes. Error bars represent standard deviations.

Figure 3 shows the imaging results from Patient 2. Similarly, significant lower rBF values (0.92 ± 0.078) were observed in the eschar volume (Fig. 3c), compared to the surrounding tissue volume (1.06 ± 0.079 , $p < 0.001$, two sample *t*-tests). Spatial variations in rBF existed across the

ROI and over different depths. Note that the wound in Patient 2 was a burn combined with a deep tissue injury, diagnosed during wound excision. In addition, the range of rBF variation in Patient 2 (0.8–1.4) was larger than that in Patient 1 (0.9–1.2).

DISCUSSION

This pilot study adapted our novel scDCT system (Fig. 1) for noncontact 3D imaging of BF distributions in burn wounds. The unique noncontact imaging technique makes it possible to image the wounds of interest without risk of infection and without interfering with sterility of the surgical field. As expected, significant lower BF values were observed in the burned/wounded volumes compared to the surrounding tissue volumes in both patients (Figs. 2 and 3). Spatial heterogeneities in rBF were also observed across different tissue volumes (eg, partial thickness burn versus full thickness burn; eschar versus noneschar) and over different depths. We noted that the rBF variation in Patient 2 (0.8–1.4) was larger than that in Patient 1 (0.9–1.2), generating a better rBF image contrast (Fig. 3b). Thus, the rBF distribution from Patient 2 (Fig. 3b) matched the pattern of the wound/eschar (Fig. 3a) better than Patient 1 (Fig. 2). The relatively smaller rBF variation/contrast across different tissue areas/volumes in Patient 1 made it more difficult to be detected. Also, it was possible that the “intact” tissue adjacent to the wound was affected by the adjacent burn. Thus, it was not surprising that lower rBF areas/volumes were observed in the “intact” tissue adjacent to the “partial thickness burn” tissue (Fig. 2). Because of the limited number of subjects in this study ($n = 2$), however, it is impossible to test the significance of inter-patient difference in rBF variations. More subjects are needed to test whether there is a minimum/maximum rBF variation that limits to clinical utility of the results.

We would like to note some limitations with the current scDCT system and study that may explain the difference of the imaging results between Patient 1 and Patient 2. Our previous studies showed that irregular tissue surface geometry can influence BF measurements and image reconstruction.¹⁴ Very recently, we integrated a novel photometric stereo technique into the scDCT system to acquire both tissue surface geometry and boundary BFI data using a single EMCCD camera.¹⁴ We are planning to adapt this modified system in patients with burn wounds to improve the quality of image reconstruction.

In addition, current data analyses assumed constant optical properties (μ_a, μ'_s) from the literature.¹⁷ This assumption may result in under- or over-estimation of rBF.^{17,18} We are currently working on new algorithms to extract μ_a, μ'_s and BFI simultaneously from the measured light intensity and speckle contrast data over multiple S-D distances.^{19–21} Although this study focuses on the 3D imaging of BF distributions, we may explore a multi-wavelength scDCT system (ie, adding more NIR laser diodes at different wavelengths) for simultaneous imaging of blood flow and oxygenation distributions to enhance the ability for assessing tissue viability.¹⁹

The sample size of this pilot study is small ($n = 2$). We plan to recruit more patients undergoing skin grafting and use scDCT to continuously monitor hemodynamic variation in targeted tissues before and after the treatment. It is anticipated that continuous monitoring of tissue blood flow/

oxygenation variations in burn wounds will provide objective information for pre-treatment planning and postoperative prediction/assessment of the intervention.

In the present study, image reconstruction and display were performed off-line. In the future, we will further develop and optimize the scDCT system with friendly graphical user interface for automatic and real-time data collection, processing, and visualization.

For imaging larger wounds, we can either enlarge the ROI or scan and assemble multiple images over larger areas. With more optimization in the future, we hope that the scDCT can be eventually used for noninvasive imaging of burn wounds in combat surgical hospitals.

CONCLUSIONS

We have adapted the innovative scDCT for 3D imaging of blood flow distributions in burn wounds. The unique noncontact 3D imaging capability makes the scDCT applicable for the imaging of the burns/wounds of interest without risk of infection and without interfering with sterility of the surgical field. Significant lower BF values were observed in the burned/wounded tissue volumes compared to the surrounding normal tissues, suggesting the potential of scDCT for diagnosis and characterizing burn wounds. In the years to come, the portable scDCT device holds the potential to be optimized and used in combat surgical hospitals to improve the acute management of battlefield burn injuries.

FUNDING

This study was partially supported by the National Institutes of Health Nos. R01-CA149274 (G. Y.), R21-AR062356 (G. Y.), and R21-HD091118 (G. Y.), American Heart Association Grant-In-Aid 16GRNT30820006 (G. Y.); National Endowment for Plastic Surgery, Plastic Surgery Foundation No. 3048112770 (L. W. and G. Y.); National Science Foundation EPSCoR #1539068 (G. Y.); and the Halcomb Fellowship in Medicine and Engineering at the University of the Kentucky (S. M.).

DISCLOSURE

G. Yu and C. Huang disclose the following patent owned by the University of Kentucky, which is related to the technology and analysis methods described in this study: G. Yu, Y. Lin, and C. Huang, “Noncontact three-dimensional diffuse optical imaging of deep tissue blood flow distribution,” US Patent #9861319 (2016 to 2036). This research was completed by co-authors unaffiliated with any commercial entity.

REFERENCES

1. Roeder RA, Schulman CI: An overview of war-related thermal injuries. *J Craniofac Surg* 2010; 21: 971–5.
2. Gurley K, Shang Y, Yu G: Noninvasive optical quantification of absolute blood flow, blood oxygenation, and oxygen consumption rate in exercising skeletal muscle. *J Biomed Opt* 2012; 17: 075010.
3. Jaskille AD, Shupp JW, Jordan MH, Jeng JC: Critical review of burn depth assessment techniques: part I. Historical review. *J Burn Care Res* 2009; 30: 937–47.

4. Zaharchuk G, Martin AJ, Dillon WP: Noninvasive imaging of quantitative cerebral blood flow changes during 100% oxygen inhalation using arterial spin-labeling MR imaging. *AJNR Am J Neuroradiol* 2008; 29: 663–7.
5. Rudroff T, Weissman JA, Bucci M, et al: Positron emission tomography detects greater blood flow and less blood flow heterogeneity in the exercising skeletal muscles of old compared with young men during fatiguing contractions. *J Physiol* 2014; 592: 337–49.
6. Takahashi S, Tanizaki Y, Kimura H, et al: Comparison of cerebral blood flow data obtained by computed tomography (CT) perfusion with that obtained by xenon CT using 320-row CT. *J Stroke Cerebrovasc Dis* 2015; 24: 635–41.
7. Trofimov AO, Kalentiev G, Voennov O, et al: Comparison of two algorithms for analysis of perfusion computed tomography data for evaluation of cerebral microcirculation in chronic subdural hematoma. *Adv Exp Med Biol* 2016; 923: 407–12.
8. Archer HA, Smailagic N, John C, et al: Regional cerebral blood flow single photon emission computed tomography for detection of frontotemporal dementia in people with suspected dementia. *Cochrane Database Syst Rev* 2015; CD010896.
9. Boas DA, Dunn AK: Laser speckle contrast imaging in biomedical optics. *J Biomed Opt* 2010; 15: 011109.
10. Jaskille AD, Ramella-Roman JC, Shupp JW, Jordan MH, Jeng JC: Critical review of burn depth assessment techniques: part II. Review of laser doppler technology. *J Burn Care Res* 2010; 31: 151–7.
11. Kim MN, Durduran T, Frangos S, et al: Noninvasive measurement of cerebral blood flow and blood oxygenation using near-infrared and diffuse correlation spectroscopies in critically brain-injured adults. *Neurocrit Care* 2010; 12: 173–80.
12. Lin Y, Huang C, Irwin D, He L, Shang Y, Yu G: Three-dimensional flow contrast imaging of deep tissue using noncontact diffuse correlation tomography. *Appl Phys Lett* 2014; 104: 121103.
13. Huang C, Irwin D, Lin Y, et al: Speckle contrast diffuse correlation tomography of complex turbid medium flow. *Med Phys* 2015; 42: 4000–6.
14. Mazdeyasna S, Huang C, Zhao M, et al: Noncontact speckle contrast diffuse correlation tomography of blood flow distributions in tissues with arbitrary geometries. *J Biomed Opt* 2018; 23: 096005.
15. Huang C, Irwin D, Zhao M, et al: Noncontact 3-D speckle contrast diffuse correlation tomography of tissue blood flow distribution. *IEEE Trans Med Imaging* 2017; 36: 2068–76.
16. Henry B, Zhao M, Shang Y, et al: Hybrid diffuse optical techniques for continuous hemodynamic measurement in gastrocnemius during plantar flexion exercise. *J Biomed Opt* 2015; 20: 125006.
17. Irwin D, Dong L, Shang Y, et al: Influences of tissue absorption and scattering on diffuse correlation spectroscopy blood flow measurements. *Biomed Opt Express* 2011; 2: 1969–85.
18. Dong L, He L, Lin Y, Shang Y, Yu G: Simultaneously extracting multiple parameters via fitting one single autocorrelation function curve in diffuse correlation spectroscopy. *IEEE Trans Biomed Eng* 2013; 60: 361–8.
19. Tamborini D, Farzam P, Zimmermann B, Wu KC, Boas DA, Franceschini MA: Development and characterization of a multidistance and multiwavelength diffuse correlation spectroscopy system. *Neurophotonics* 2018; 5: 011015.
20. Liu J, Zhang H, Lu J, Ni X, Shen Z: Simultaneously extracting multiple parameters via multi-distance and multi-exposure diffuse speckle contrast analysis. *Biomed Opt Express* 2017; 8: 4537–50.
21. Valdes CP, Varma HM, Kristoffersen AK, Dragojevic T, Culver JP, Durduran T: Speckle contrast optical spectroscopy, a non-invasive, diffuse optical method for measuring microvascular blood flow in tissue. *Biomed Opt Express* 2014; 5: 2769–84.